



Drying kinetics of tobacco strips at different air temperatures and relative humidities

Y. N. Xin¹ · J. W. Zhang¹ · B. Li²

Received: 17 August 2017 / Accepted: 15 January 2018 / Published online: 1 February 2018
© Akadémiai Kiadó, Budapest, Hungary 2018

Abstract

The effects of air temperature and relative humidity (RH) on the drying kinetics of two kinds of flue-cured tobacco strips (C3F and B3F) were studied using a thermogravimetric device in this work. The drying experiments were carried out with drying air temperatures of 60, 70, 80, and 90 °C and RH values of 0, 10, 20, 30, and 40% at a constant airflow. Taking the effect of RH into consideration, a modified Arrhenius-type equation of diffusivity was proposed. In addition, comparing five thin-layer drying models and five equilibrium moisture content models to describe the drying kinetics and the desorption isotherms of tobacco strips, high coefficients of determination (R^2) and low reduced Chi-square (χ^2) and residual sum of squares (RSS) values indicated that the Logarithmic model and the Modified Oswin model appeared to be the most suitable for predicting the moisture ratio and the moisture desorption relationship of tobacco strips. The effective moisture diffusion coefficient under different temperatures and RHs ranged from 1.68×10^{-11} to $6.81 \times 10^{-11} \text{ m}^2 \text{ s}^{-1}$ for C3F and from 1.62×10^{-11} to $6.68 \times 10^{-11} \text{ m}^2 \text{ s}^{-1}$ for B3F. A modified Arrhenius-type equation with an RH term was found to be effective for describing the drying behavior of two flue-cured tobacco strips, and the activation energy (E_a) values were 34.6 and 35.2 kJ mol^{-1} for C3F and B3F, respectively.

Keywords Flue-cured tobacco · Drying kinetics · Temperature · Relative humidity · Diffusion

List of symbols

A	Model constant (–)
a, b, c, k, n	Model constant (–)
B_1	Constant ($\text{m}^2 \text{ s}^{-1}$)
B_2	Constant ($\%^{-1}$)
D_{eff}	Effective diffusion coefficient of moisture ($\text{m}^2 \text{ s}^{-1}$)
DR	Drying rate (dry basis) ($\text{g water g}^{-1} \text{ s}^{-1}$)
E_a	Activation energy (kJ mol^{-1})
L	Average thickness of tobacco strips (m)
MR	Moisture ratio (–)
$\text{MR}_{\text{exp},i}$	The i -th experimental moisture ratio (–)
$\text{MR}_{\text{pre},i}$	The i -th predicted moisture ratio (–)

N	Number of observations (–)
n	Number of constants (–)
R	Gas constant ($\text{J mol}^{-1} \text{ K}^{-1}$)
R^2	Coefficient of determination (–)
RSS	Residual sum of squares (–)
RH	Relative humidity (%)
T	Temperature (°C)
t	Time (s)
X	Moisture content (dry basis) (g water g^{-1})
χ^2	Reduced Chi-square (–)

Subscripts

0	Initial value
e	Equilibrium

✉ J. W. Zhang
zhangjw@mail.buct.edu.cn

✉ B. Li
lib@ztri.com.cn

¹ College of Chemical Engineering, Beijing University of Chemical Technology, Beijing 100029, China

² Key Laboratory of Tobacco Processing Technology, Zhengzhou Tobacco Research Institute, Zhengzhou 450001, China

Introduction

Tobacco is well-known as an important economical crop in Chinese agriculture. Tobacco leaves have a very complex biomass matrix [1], and their threshing and redrying processes the transitional phase between agricultural product process and cigarette production in modern cigarette

production process. Because of its moisture desorption property, tobacco is reprocessed to make it suitable for storage and to conform further to the requirements of cigarette manufacturing. Hot air dehydration by convection is an important operation in the tobacco threshing and redrying process, involving with complex phenomena of heat and mass transfer under certain temperature and humidity conditions. In this process, air temperature and relative humidity (RH) are two important factors that affect the drying characteristics of tobacco strips.

As discussed in previous works, various studies have reported the drying kinetics of fruits [2, 3], vegetables [4], and other products, such as municipal sewage sludge [5], wood [6], sage leaves [7], and grape seeds [8]. Meanwhile, studies on the drying of tobacco raw materials have focused mainly on the flue-curing process [9–11] with temperatures between 20 and 70 °C, the drying progress of cut tobacco [12–14], and the humidifying process of tobacco strips [15, 16]. However, there have been few reports about the drying kinetics of tobacco strips under different conditions of threshing and redrying temperature and humidity. In addition, during tobacco-redrying process, it is essential to have moisture desorption isotherm data because these data can provide an estimate of the minimum moisture content that can be attained under certain temperature and RH conditions. Furthermore, the difference between the moisture content and the equilibrium moisture content is the driving force for redrying, and it directly affects the moisture migration speed.

The drying kinetics of tobacco strips or similar biomass are mainly based on the data derived from experiments and diffusion theory. The drying kinetics of biological materials is a complex phenomenon and requires dependable models to describe drying behavior. The applicabilities of these models are usually based on the agreement between the experimental results and the resulting residuals of the fit plots [17]. Lewis [18], Page [19], Henderson and Pabis [20], modified Page [21], and Logarithmic [2] models are commonly used to describe the drying characteristics of biological materials. Moreover, Henderson [22], Modified Henderson [23], Modified Chung-Pfost [24], Halsey [25], and Modified Oswin [26] models are the common equilibrium moisture content models.

In this study, the features of drying kinetics of two flue-cured tobacco strips were studied using an online thermogravimetric device. Drying experiments were carried out under various air temperatures (60–90 °C) and RH levels (0–40%). The purpose of this study was to reveal the effects of drying air temperature and RH on the effective diffusion coefficient and activation energy to improve understanding on the drying behavior of flue-cured tobacco strips. Moreover, using the experimental data, the most appropriate thin-layer drying model and desorption equilibrium

moisture content model were determined through nonlinear regression analysis.

Materials and methods

Sample preparation

The experimental materials—upper tobacco strips (B3F) & middle tobacco strips (C3F), obtained in 2011 from Sanmenxia area (one of the most suitable planting areas for high-quality flue-cured tobacco in China), were chosen after separated from tobacco stems in the threshing process. Comparing with B3F, the leaf structure and thickness of C3F are unconsolidated and thin, respectively, meanwhile the flavor and nicotine quantity supplied by C3F are less.

The initial moisture contents of the raw materials were measured by the oven method. Water was added to the samples, with the amount being determined by the conservation of mass during the humidification process. The selected raw materials were uniformly humidified to a moisture content of 33% (dry basis) in isothermal and constant humidity equipment [13].

Experimental apparatus and procedure

The experimental devices shown in Fig. 1 mainly consisted of a temperature and humidity preprocessing system and a measuring system. The temperature and humidity preprocessing system included a mass flowmeter (2), a pump (3), a saturated steam generator (4), a preheater and stream generator (5), and a mixer (6). This system can change the air temperature from room temperature to 300 °C, relative humidity from 0 to 100%, and airflow velocity from 0 to 0.1 m s⁻¹. The measuring system mainly included a tubular furnace (7), surface temperature and weight sensors (8), and a data acquisition system (9). The data acquisition system had a capacity of 0–200 g and accuracy of 0.1 mg, and it was connected to a computer so that the weights and temperatures of the samples during drying could be recorded continuously.

For the requirements of the thin-layer drying process and the elimination of external diffusion, the air velocity was set at 0.06 m s⁻¹ to obtain the real and effective diffusion coefficients [27]. The samples were dehydrated from an initial moisture content of 33% (dry basis) to the equilibrium moisture content under the drying conditions. The drying characteristics of tobacco strips were investigated by changing the ambient temperature from 60 to 90 °C and the relative humidity from 0 to 40%. The experiments were repeated at least three times to validate the results obtained.

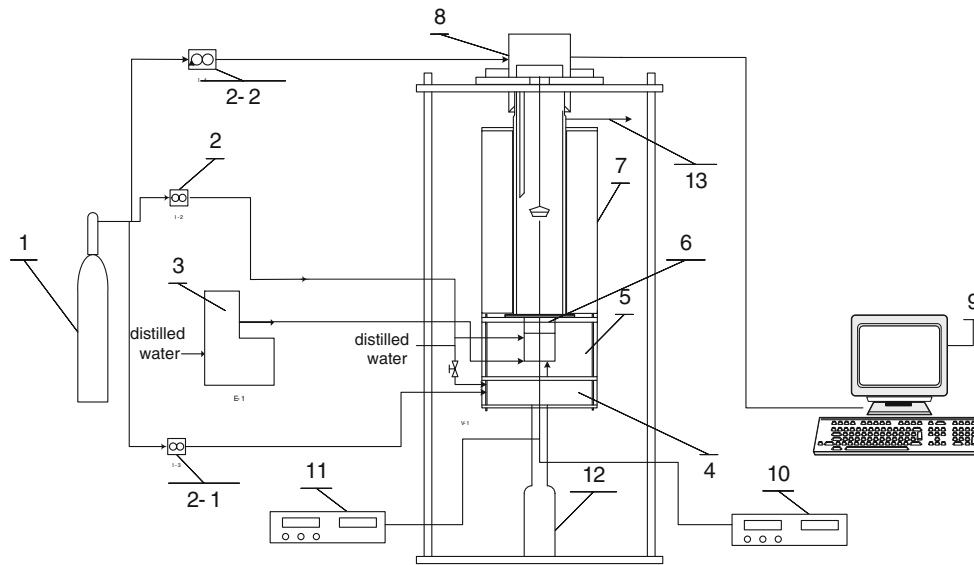


Fig. 1 TG drier: 1. Compressed air or N₂; 2. Mass flowmeter; 3. Pump; 4. Saturated steam generator; 5. Preheater and stream generator; 6. Mixer; 7. Tubular furnace; 8. Surface temperature and

weight sensors; 9. Data acquisition system; 10. Intelligent temperature controller; 11. Temperature controller; 12. Hydraulic lifter; 13. Outlet

Mathematical modeling

The moisture ratio (MR) during drying experiments was calculated by using the following equation:

$$MR = \frac{(X - X_e)}{(X_0 - X_e)} \tag{1}$$

where X indicates the moisture content (dry basis), g water g⁻¹; X_0 denotes the initial moisture content (dry basis), g water g⁻¹; and X_e denotes the equilibrium moisture content (dry basis), g water g⁻¹.

The drying rate (DR) of tobacco strips could be expressed as the ratio of water loss and time:

$$DR = - \frac{X_{t+\Delta t} - X_t}{\Delta t} \tag{2}$$

where DR is drying rate (dry basis), g water g⁻¹ s⁻¹; X_t and $X_{t + \Delta t}$ are the moisture contents at t and $t + \Delta t$, respectively; and t is the drying time, s.

To explore the drying behaviors of two kinds of flue-cured tobacco (C3F and B3F) under the specified conditions, the drying experimental data were fitted to five equilibrium moisture content equations (Table 1) and five commonly used thin-layer drying models (Table 4). To evaluate the performance of the models, the determination coefficients (R^2), the reduced Chi-square (χ^2), and the residual sum of squares (RSS) were calculated. χ^2 and RSS can be calculated as follows [28, 29]:

$$\chi^2 = \frac{\sum_{i=1}^n (MR_{exp,i} - MR_{pre,i})^2}{N - n} \tag{3}$$

Table 1 Equilibrium moisture content models

Model	Model equation
Henderson	$X_e = \left[\frac{\ln(1-RH/100)}{-aT} \right]^{\frac{1}{b}}$
Modified Henderson	$X_e = \left[\frac{\ln(1-RH/100)}{-a(T+c)} \right]^{\frac{1}{b}}$
Modified Chung-Pfost	$X_e = -\frac{1}{b} \ln \left(\frac{(T+c)}{-a} \ln \left(\frac{RH}{100} \right) \right)$
Halsey	$X_e = \left[\frac{\exp(aT+c)}{-\ln \left(\frac{RH}{100} \right)} \right]^{\frac{1}{b}}$
Modified Oswin	$X_e = (a + bT) \left(\frac{RH/100}{1 - RH/100} \right)^c$

$$RSS = \sum_{i=1}^N (MR_{pre,i} - MR_{exp,i})^2 \tag{4}$$

where $MR_{exp, i}$ and $MR_{pre, i}$ are experimental and predicted moisture ratios, respectively; N is the number of observations; and n is the number of constants.

Effective moisture diffusivity

The convective drying of tobacco is a complicated heat and mass transfer process, and the mass transport was considered to be one-dimensional since the thickness of samples (0.3 mm) was much smaller than its width and length. In this study, the external resistance to mass transfer was assumed to be negligible, the effective moisture diffusivity to be constant, and the solid tobacco strips to be isotropic

and homogeneous. The mass transfer process can be described by Fick's second law as follows:

$$\frac{\partial X}{\partial t} = D_{\text{eff}} \frac{\partial^2 X}{\partial x^2} \left(-L/2 \leq x \leq L/2 \right) \quad (5)$$

where D_{eff} denotes the effective diffusion coefficient of moisture, $\text{m}^2 \text{s}^{-1}$; x is the diffusion path, m ; and L is the average thickness of tobacco strips, m .

The solution of Eq. (5) in infinite slabs was given by Crank [30] as shown in Eq. (6), assuming negligible external resistance to mass transfer, uniform initial moisture content and temperature, and negligible shrinkage:

$$\text{MR} = \frac{8}{\pi^2} \sum_{n=1}^{\infty} \frac{1}{(2n-1)^2} \exp\left(-\frac{(2n-1)^2 \pi^2 D_{\text{eff}} t}{L^2}\right) \quad (6)$$

Various researchers have used only the first term of the series given in Eq. (6) to describe changes in moisture content [31–33]. However, the first term of Eq. (6) was not sufficiently accurate to predict the moisture contents of tobacco strips according to the experimental data that we obtained from this study, since using the first term yielded smaller R^2 and larger χ^2 and RSS values than the first two or more terms by nonlinear regression analysis. Thus, Eq. (6) was modified by the first two terms of the series as:

$$\text{MR} = \frac{8}{\pi^2} \exp\left(-\frac{\pi^2 D_{\text{eff}} t}{L^2}\right) + \frac{8}{9\pi^2} \exp\left(-\frac{9\pi^2 D_{\text{eff}} t}{L^2}\right) \quad (7)$$

The effective diffusivity was typically obtained by fitting experimental data in terms of MR against drying time t in Eq. (7).

Results and discussion

Equilibrium moisture contents

Drying continued until the moisture content had changed by less than 0.3% since the previous measurement, and the equilibrium moisture contents of C3F and B3F at various temperatures and RH were thus obtained. The desorption isotherms representing the responses of the moisture content to temperatures and RH are illustrated in Fig. 2.

The equilibrium moisture contents of C3F and B3F increased with decreasing temperature and with increasing RH. For instance, as temperature decreased from 80 to 70 °C, the C3F adsorbed an additional 0.4% (dry basis) of moisture with RH kept constant at 10%. This occurred mainly because the attractive forces between water molecules decreased with increasing temperature, and the water molecules were in a higher active state. This result is consistent with similar results for other leaves that have been reported by Ait et al. [34], Argyropoulos et al. [35],

and Mghazli et al. [36]. At higher temperatures, temperature had less influence on the equilibrium moisture content than did RH.

It also can be seen from Fig. 2 that the equilibrium moisture content of C3F is basically higher than that of B3F in the same temperature and RH condition, and the difference between C3F and B3F increases with the increasing of RH. The main reason is that the hydrophilic colloid and water-soluble crystalline materials in C3F are more than those in B3F.

Five commonly used semiempirical models, as described in Table 1, were tested for their effectiveness in fitting the experimental desorption isotherm data. Tables 2 and 3 list the model coefficients and the relevant statistics of C3F and B3F, respectively. For the same dataset, the model with the highest R^2 and the smallest χ^2 and RSS values was used to provide the best fitness. The five moisture desorption isotherm models all fitted well with the experimental data for both flue-cured tobacco strips. However, due to the fact that lower χ^2 and RSS values were obtained from the Modified Oswin model than the other four models, the Modified Oswin model was proved to be the most appropriate model to describe the moisture desorption relationship for both flue-cured tobacco strips. Similar results have been reported by Raji et al [23] and He et al. [37], who proposed the Modified Oswin model as the most appropriate model to describe their sorption isotherms.

Effect of temperature on drying characteristics of tobacco

The drying characteristic curves of C3F and B3F under temperatures of 60, 70, 80, and 90 °C at constant 30% RH are shown in Fig. 3. As expected, the MR decreased with increasing drying time. Obviously, all the curves appeared to have two drying stages. The MR decreased rapidly during the initial drying process and decreased slowly later. The effect of temperature on drying was significant, and the higher the temperature was, the higher the rate of reduction in moisture content was. The drying time required to reduce to the desired moisture content was influenced by temperature, being highest at 60 °C and lowest at 90 °C. For C3F to be dried to a final moisture ratio of 0.2, the times required at 60, 70, 80, and 90 °C were 618, 472, 315, and 242 s, respectively. For B3F, the required times were 635, 473, 298, and 244 s, respectively. Similar results were also observed in the drying of fruits [2] and vegetables [4].

The drying rates, as functions of the moisture content (dry basis), during the drying process for C3F and B3F under various temperatures at 30% RH are given in Fig. 4. As indicated, a period of constant drying rate did not occur, but the drying curves exhibited a falling rate period except

Fig. 2 Equilibrium moisture content curves of C3F (a) and B3F (b)

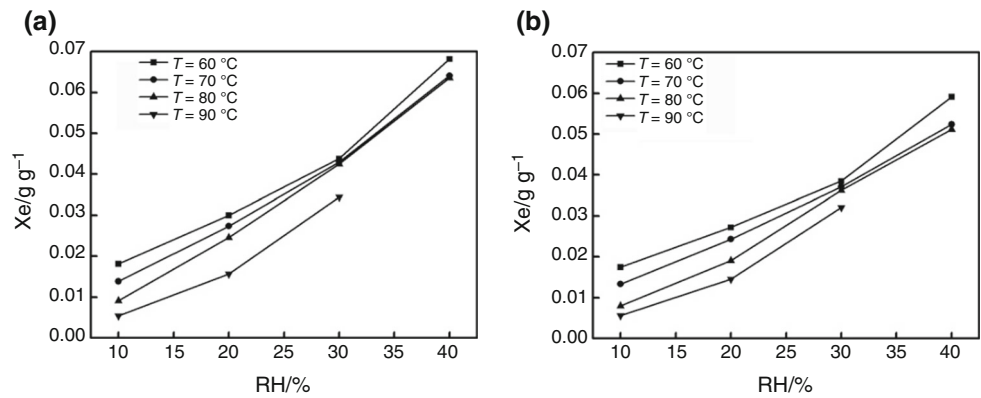


Table 2 Different model fitting results of equilibrium moisture content of C3F

Model	Model parameters			R^2	χ^2	RSS
	a	b	c			
Henderson	0.01572	0.86258	/	0.96606	1.49×10^{-5}	2.09×10^{-4}
Modified Henderson	0.02837	0.87395	- 147.94252	0.96686	1.45×10^{-5}	1.89×10^{-4}
Modified Chung-Pfost	455.1264	17.59664	- 176.00259	0.9452	2.41×10^{-5}	3.13×10^{-4}
Halsey	- 0.00335	0.57207	- 0.48777	0.96867	1.38×10^{-5}	1.79×10^{-4}
Modified Oswin	0.28928	- 5.57391×10^{-4}	0.97536	0.96935	1.35×10^{-5}	1.75×10^{-4}

Table 3 Different model fitting results of equilibrium moisture content of B3F

Model	Model parameters			R^2	χ^2	RSS
	a	b	c			
Henderson	0.02317	0.93951	/	0.95697	1.23×10^{-5}	1.72×10^{-4}
Modified Henderson	0.06436	0.96228	- 212.324	0.96732	9.32×10^{-6}	1.21×10^{-4}
Modified Chung-Pfost	381.7775	21.91207	- 209.58995	0.95795	1.20×10^{-5}	1.56×10^{-4}
Halsey	- 0.00487	0.62406	- 0.21986	0.96669	9.50×10^{-6}	1.23×10^{-4}
Modified Oswin	0.27884	- 5.82808×10^{-4}	0.88893	0.96846	8.99×10^{-6}	1.17×10^{-4}

for a very short accelerating period at the start. Drying rates increased at the start due to the adaptation of the materials to the drying medium and the ease of removal of free water from the material [38]. The falling rate period was controlled by diffusion [39]. These results were consistent with previous observations on drying various food and raw materials [40, 41].

Furthermore, as shown in Fig. 4, the drying rate increased with rising air temperature at a constant RH. When the moisture content decreased to 0.1 (dry basis), the average values of DR at 60, 70, 80, and 90 °C were 3.77×10^{-4} , 4.94×10^{-4} , 7.40×10^{-4} , and 9.63×10^{-4} g water g⁻¹ s⁻¹ and 3.67×10^{-4} , 4.93×10^{-4} , 7.82×10^{-4} , and 9.55×10^{-4} g water g⁻¹ s⁻¹ of C3F and

B3F, respectively. When at 20% RH, the maximum drying rate at 90 °C was nearly three times greater than that at 60 °C for C3F and B3F.

Effect of humidity on characteristics of tobacco drying

The drying characteristic curves of C3F and B3F under RHs of 0, 10, 20, 30, and 40% at 60 °C are shown in Fig. 5. It can be seen that the MR decreased with drying time. The effect of humidity on drying was significant, and the lower the RH was, the higher the rate of reduction in moisture content was. The drying time required to reach the desired moisture content was influenced by RH, being highest at

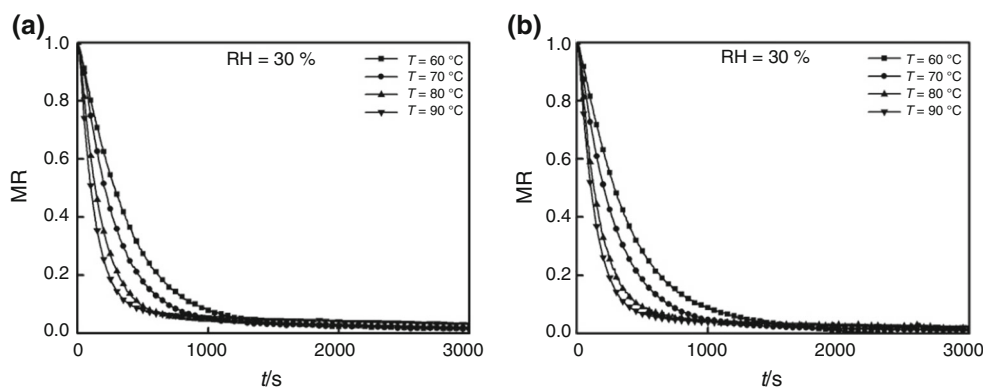
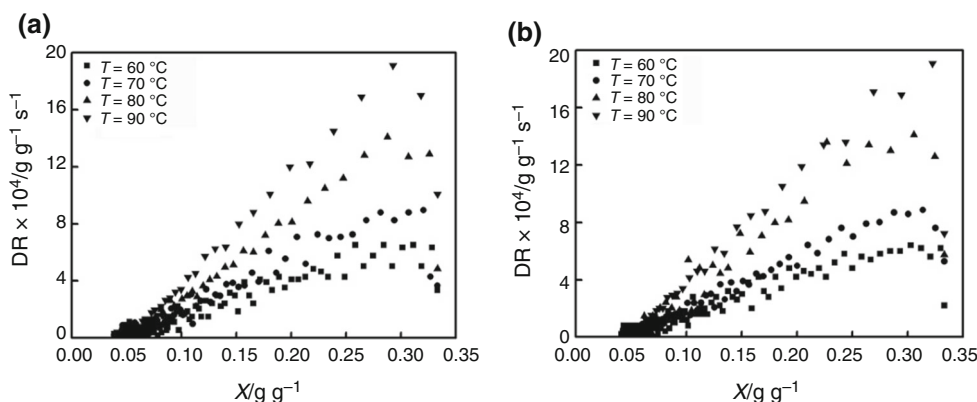


Fig. 3 Drying curves of C3F (a) and B3F (b) under different temperatures at 30% RH

Fig. 4 Drying rate versus moisture content of C3F (a) and B3F (b) under different temperatures at 30% RH



40% and lowest at 0%. For C3F, to dry the material to a final moisture ratio of 0.2, the times required at 0, 10, 20, 30, and 40% were 532, 589, 598, 621, and 727 s, respectively. For B3F, the required times were 510, 567, 594, 636, and 786 s, respectively. These results were also consistent with the observations of Inazu et al. [42] and Villeneuve et al. [43].

Furthermore, it can be seen from Fig. 6 that the drying rate decreased with increasing RH at a constant temperature. This may be because the increase in RH led to an increase in the equilibrium moisture content, decreasing the driving force of drying. When the moisture content decreased to 0.1 (dry basis), the average values of DR at RHs of 0, 10, 20, 30, and 40% were 4.39×10^{-4} , 3.96×10^{-4} , 3.9×10^{-4} , 3.76×10^{-4} , and 3.21×10^{-4} g water $\text{g}^{-1} \text{s}^{-1}$ and 4.58×10^{-4} , 4.12×10^{-4} , 3.93×10^{-4} , 3.67×10^{-4} , and 2.97×10^{-4} g water $\text{g}^{-1} \text{s}^{-1}$ for C3F and B3F, respectively. When at 90 °C, the maximum drying rate from 40% RH to 0% RH increased by approximately 50% for both C3F and B3F.

Evaluation of drying models

Nonlinear regression analyses were carried out, and the fittings obtained are illustrated for one drying test with 10%

RH and 90 °C. Similar results were obtained for all of the considered drying conditions investigated. The thin-layer drying models utilized are listed in Table 4, and corresponding model constants and curve-fitting results are shown in Tables 5 and 6 for C3F and B3F, respectively. As seen in these tables, all five drying models yielded excellent fitting results for the experimental data, with R^2 values higher than 0.97 and 0.98 for C3F and B3F, respectively. In general, values of R^2 , χ^2 , and RSS varied from 0.9774 to 0.9987, 0.0000589 to 0.00102, and 0.007664 to 0.031976, respectively. Furthermore, among the five drying models, the highest values of determination coefficients ($R^2 > 0.998$) and the lowest values of χ^2 and RSS indicated that the Logarithmic model was the most suitable model for all drying conditions. This result was in agreement with drying of jujube slices [44] and apricots [45, 46].

The model coefficients and exponents of the Logarithmic model obtained by nonlinear regressions are given in Tables 7 and 8, which show that the Logarithmic model was suitable for all the experimental data. In addition, the comparison between experimental and predicted MR values using the Logarithmic model at different temperatures and RHs is shown in Fig. 7. The predicted data generally banded around a 45° straight line, which shows that the

Fig. 5 Drying curves of C3F (a) and B3F (b) at 60 °C with different air relative humidities

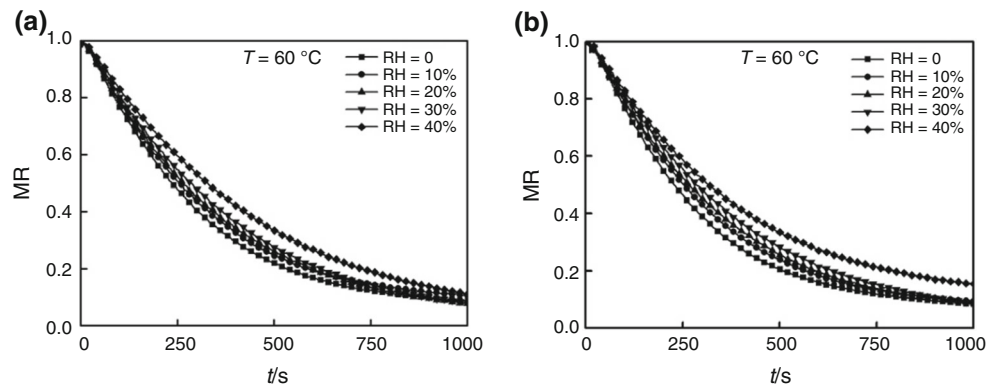
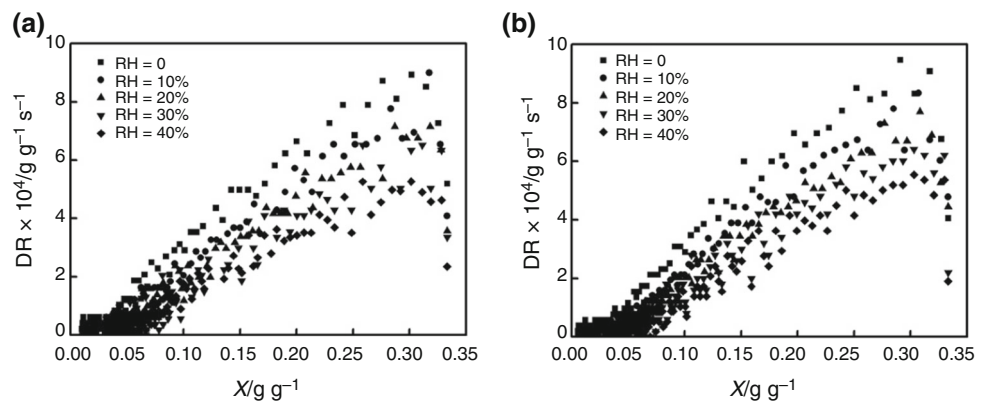


Fig. 6 Drying rates of C3F (a) and B3F (b) at 60 °C with different air relative humidities



Logarithmic model is suitable for describing the thin-layer drying characteristics of two kinds of tobacco strips.

Effective diffusion coefficient and activation energy

The effective diffusion coefficients for C3F and B3F tobacco strips under different temperatures and RHs were estimated using Eq. (7) by nonlinear regression and are shown in Tables 9 and 10, respectively. The effective diffusion coefficient for C3F tobacco was $(1.68\text{--}6.81) \times 10^{-11} \text{ m}^2 \text{ s}^{-1}$, and the coefficient for B3F tobacco was $(1.62\text{--}6.68) \times 10^{-11} \text{ m}^2 \text{ s}^{-1}$. It can be seen from Tables 9 and 10 that the values of D_{eff} increased with increasing drying temperature and decreasing RH of drying air. The moisture-effective diffusivities obtained from the present study are similar to those found by Panchariya et al.

[47] in the case of black tea, in which values ranged from 1.14×10^{-11} to $2.98 \times 10^{-11} \text{ m}^2 \text{ s}^{-1}$.

The values obtained in the present study are lower than reported diffusivities for apricot pomace [3] dried at temperatures ranging from 40 to 70 °C, which varied from 1.01×10^{-9} to $1.86 \times 10^{-9} \text{ m}^2 \text{ s}^{-1}$. In addition, moisture-effective diffusivity values for garden mint leaves [48] varied from 4.77×10^{-13} to $2.95 \times 10^{-12} \text{ m}^2 \text{ s}^{-1}$. These differences could be caused by differences in the biomaterial structures, the drier conditions, the drying methods, the mathematic model for the D_{eff} , and other factors.

In addition, the effects of air temperature [49–51] and the effective diffusivity were always described by an Arrhenius-type relationship to obtain better agreement between the predicted and the experimental data, as shown below:

$$D_{\text{eff}} = A \exp\left(-\frac{E_a}{R(T + 273.15)}\right) \tag{8}$$

Then, the natural logarithmic of D_{eff} can be written as

$$\ln D_{\text{eff}} = \ln A - \frac{E_a}{R(T + 273.15)} \tag{9}$$

Figure 8 shows the relationship between $\ln D_{\text{eff}}$ in Eq. (9) and $\text{RH}/100$ under certain temperature, and $\ln D_{\text{eff}}$ is approximately linear with $\text{RH}/100$, indicating that $\ln A$ in

Table 4 Thin-layer drying models

Model	Model equation
Lewis	$\text{MR} = \exp(-kt)$
Page	$\text{MR} = \exp(-kt^n)$
Henderson and Pabis	$\text{MR} = a \exp(-kt)$
Modified page	$\text{MR} = \exp(-(kt)^n)$
Logarithmic	$\text{MR} = a \exp(-kt) + c$

Table 5 Results of statistical analyses on the modeling of C3F drying at 10% RH with 90 °C

Model	C3F model constants	R^2	χ^2	RSS
Lewis	$k = 0.00762$	0.9774	0.00102	0.03197
Page	$k = 0.00922; n = 0.96173$	0.9779	0.001	0.03163
Henderson and Pabis	$a = 1.03614; k = 0.0792$	0.9782	0.000987	0.03138
Modified page	$k = 0.0766; n = 0.95217$	0.9779	0.001	0.03161
Logarithmic	$a = 1.02355; k = 0.00939;$	0.9983	0.0000752	0.008657

Table 6 Results of statistical analyses on the modeling of B3F drying at 10% RH with 90 °C

Model	B3F model constants	R^2	χ^2	RSS
Lewis	$k = 0.00784$	0.9872	0.000592	0.024319
Page	$k = 0.00736; n = 1.01256$	0.9872	0.000594	0.024341
Henderson and Pabis	$a = 1.04688; k = 0.0823$	0.9886	0.00053	0.022993
Modified page	$k = 0.0784; n = 1.00249$	0.9872	0.000593	0.024318
Logarithmic	$a = 1.05048; k = 0.00926;$	0.9987	0.0000589	0.007664

Table 7 Logarithmic model fitting results of equilibrium moisture content of C3F

$T/^\circ\text{C}$	RH/%	Model constants			R^2	χ^2	RSS
		a	k	c			
60	0	1.00585	0.00341	0.04492	0.999	6.67×10^{-5}	0.008155
	10	0.99322	0.0032	0.05564	0.99897	6.73×10^{-5}	0.008193
	20	1.02676	0.00279	0.00932	0.99968	2.17×10^{-5}	0.004653
	30	1.04791	0.00256	-0.00905	0.99948	3.64×10^{-5}	0.006024
	40	1.04379	0.00219	-0.01121	0.99973	1.81×10^{-5}	0.00425
70	0	1.00695	0.00505	0.04075	0.99885	7.00×10^{-5}	0.008353
	10	1.02408	0.00443	0.03763	0.99908	6.07×10^{-5}	0.007778
	20	1.04241	0.00408	0.03797	0.99802	1.39×10^{-4}	0.011764
	30	1.04481	0.00374	0.0222	0.99911	6.34×10^{-5}	0.007951
	40	1.00351	0.00332	0.03076	0.99977	1.50×10^{-5}	0.003865
80	0	1.05032	0.00814	0.02731	0.99855	7.38×10^{-5}	0.00858
	10	1.05288	0.00756	0.03194	0.99862	7.38×10^{-5}	0.00858
	20	1.05814	0.00662	0.03125	0.99856	8.46×10^{-5}	0.009185
	30	1.02753	0.00596	0.04394	0.99933	3.95×10^{-5}	0.006271
	40	1.03625	0.00522	0.03744	0.99922	4.98×10^{-5}	0.00705
90	0	1.01464	0.01165	0.04527	0.9971	1.05×10^{-4}	0.010239
	10	1.04339	0.00939	0.04105	0.99834	7.52×10^{-5}	0.008657
	20	1.02355	0.00892	0.05382	0.99891	4.93×10^{-5}	0.007011
	30	1.01166	0.00807	0.05878	0.99933	3.19×10^{-5}	0.005637

Eq. (9) could be represented by the following linear function of RH:

$$\ln A = \ln B_1 + B_2 \frac{RH}{100} \quad (10)$$

Thus, combined Eqs. (9) and (10), the corrective relationship between the moisture-effective diffusion coefficient and the comprehensive influence of air temperature and RH can be written as [42]

$$D_{\text{eff}} = B_1 \exp\left(-\frac{E_a}{R(T + 273.15)} + B_2 \frac{RH}{100}\right) \quad (11)$$

The activation energy (E_a) was obtained as presented in Eq. (11). Thus, considering the influence of air temperature and RH for C3F and B3F and using a nonlinear regression method, the model parameters of Eq. (11) and R^2 are shown in Table 11. The activation energy (E_a) values were found to be 34.6 and 35.2 kJ mol⁻¹ for C3F and B3F, respectively. The activation energy of C3F is slightly smaller than that of B3F, and from the results described above, comparing the drying rate and effective moisture diffusivities, the differences of drying characteristics between CF3 and B3F are small and the regularity is not so

Table 8 Logarithmic model fitting results of upper strips equilibrium moisture content of B3F

$T/^\circ\text{C}$	RH/%	Model constants			R^2	χ^2	RSS
		a	k	c			
60	0	1.01487	0.00362	0.0496	0.99859	9.50×10^{-5}	0.009733
	10	1.01487	0.00318	0.04031	0.99872	8.69×10^{-5}	0.009309
	20	1.02235	0.00288	0.02108	0.99933	4.56×10^{-5}	0.006745
	30	1.02235	0.00258	0.00156	0.99944	3.90×10^{-5}	0.006239
	40	0.96977	0.00258	0.07335	0.99944	3.36×10^{-5}	0.00579
70	0	0.96977	0.00554	0.09391	0.9983	9.28×10^{-5}	0.009617
	10	1.00504	0.00477	0.06072	0.99895	6.50×10^{-5}	0.00805
	20	1.00504	0.00437	0.06213	0.99897	6.59×10^{-5}	0.008103
	30	1.01951	0.00363	0.01961	0.99977	1.55×10^{-5}	0.003926
	40	1.01951	0.00313	0.00651	0.99964	2.56×10^{-5}	0.005054
80	0	1.07192	0.00825	0.0366	0.99702	1.57×10^{-4}	0.012497
	10	1.07192	0.00825	0.06784	0.99702	1.47×10^{-4}	0.012092
	20	1.04759	0.0071	0.04028	0.99839	8.89×10^{-5}	0.009414
	30	1.04759	0.00626	0.04546	0.99892	6.24×10^{-5}	0.007887
	40	1.03102	0.0057	0.0464	0.99896	6.27×10^{-5}	0.007907
90	0	1.03102	0.01144	0.04426	0.99659	1.27×10^{-4}	0.011255
	10	1.05048	0.00926	0.02938	0.99873	5.89×10^{-5}	0.007664
	20	1.05048	0.0081	0.0452	0.99942	2.75×10^{-5}	0.005238
	30	1.03297	0.0076	0.04259	0.99924	3.92×10^{-5}	0.006252

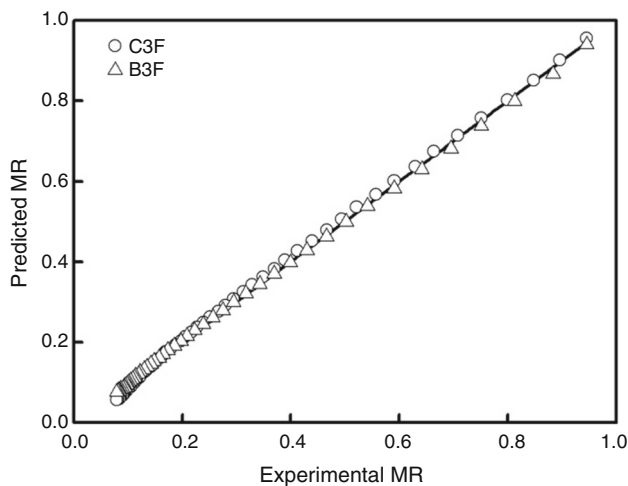


Fig. 7 Experimental MR versus Predicted MR for the Logarithmic model

obvious. This phenomenon may be explained by that the differences in appearance characteristics and chemical materials in the two tobacco strips have little influence on the drying characteristics in the work.

The activation energy values obtained in the present study are consistent with the values reported for other biological materials: apricot halves [38] (35.9 kJ mol^{-1} on average) and garlic [52] (30.6 kJ mol^{-1} on average). These values are higher than the activation energy of sweet potato slice drying [53] (ranging from 22.7 to 23.2 kJ mol^{-1}) and lower than the activation energy of sour cherry drying [40] (ranging from 64.4 to 66.1 kJ mol^{-1}).

The calculated values of moisture-effective diffusion coefficients for C3F and B3F were compared with the corresponding experimental data in Fig. 9. It can be seen from this plot that the data lie around a line with a 45° slope. Therefore, Eq. (11) describes the relationship

Table 9 Effective moisture diffusivity for C3F tobacco at different temperatures and RHs

Temperature $T/^\circ\text{C}$	$D_{\text{eff}}/\text{m}^2 \text{ s}^{-1}$				
	RH = 0%	RH = 10%	RH = 20%	RH = 30%	RH = 40%
60	2.11×10^{-11}	1.92×10^{-11}	1.91×10^{-11}	1.81×10^{-11}	1.68×10^{-11}
70	3.15×10^{-11}	2.77×10^{-11}	2.51×10^{-11}	2.43×10^{-11}	2.17×10^{-11}
80	5.11×10^{-11}	4.66×10^{-11}	4.09×10^{-11}	3.58×10^{-11}	3.22×10^{-11}
90	6.81×10^{-11}	5.56×10^{-11}	5.03×10^{-11}	4.50×10^{-11}	–

Table 10 Effective moisture diffusivity for B3F tobacco at different temperatures and RHs

Temperature $T/^\circ\text{C}$	$D_{\text{eff}}/\text{m}^2 \text{ s}^{-1}$				
	RH = 0%	RH = 10%	RH = 20%	RH = 30%	RH = 40%
60	2.18×10^{-11}	1.98×10^{-11}	1.90×10^{-11}	1.77×10^{-11}	1.62×10^{-11}
70	2.80×10^{-11}	2.75×10^{-11}	2.51×10^{-11}	2.44×10^{-11}	2.15×10^{-11}
80	4.88×10^{-11}	4.30×10^{-11}	4.22×10^{-11}	3.71×10^{-11}	3.08×10^{-11}
90	6.68×10^{-11}	5.76×10^{-11}	4.82×10^{-11}	4.52×10^{-11}	–

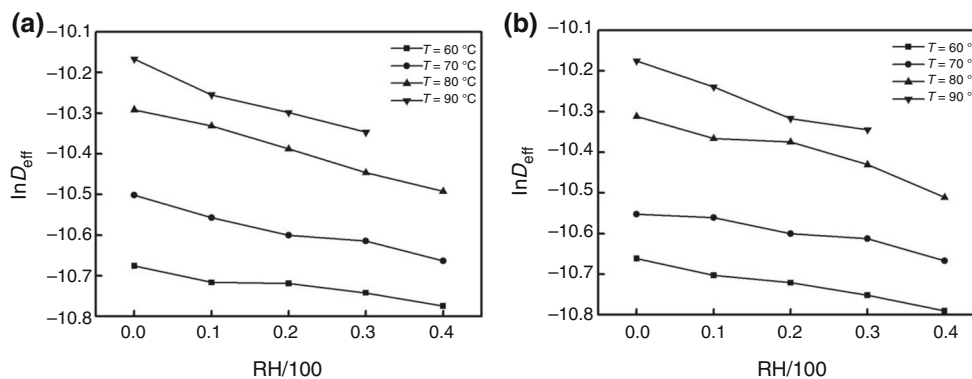


Fig. 8 Relationships between $\ln D_{\text{eff}}$ in Eq. (9) and RH/100: **a** C3F; and **b** B3F

Table 11 Results calculated by Eq. (11)

Parameter	C3F	B3F
$E_a/\text{kJ mol}^{-1}$	34.6	35.2
$B_1/\text{m}^2 \text{ s}^{-1}$	6.34×10^{-6}	7.48×10^{-6}
$B_2/\%^{-1}$	– 1.12826	– 1.04494
R^2	0.97298	0.97185

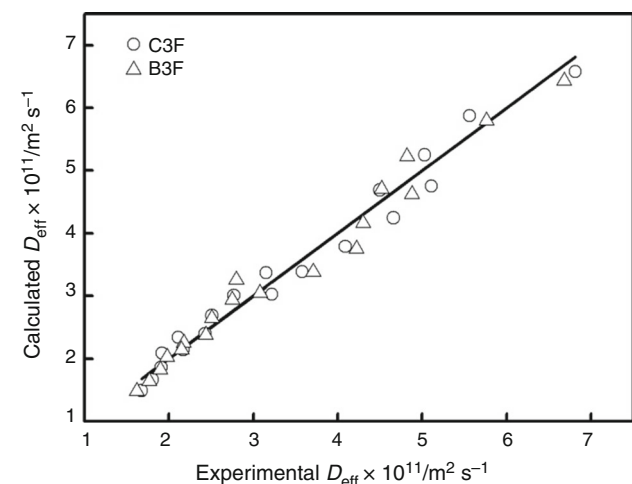


Fig. 9 Comparison of moisture-effective diffusion coefficients between calculated and experimental data

between the diffusion coefficient and the effects of temperature and RH on tobaccos well.

Conclusions

Drying experiments were carried out to explore the drying kinetics of two kinds of tobacco under various temperature and relative humidity conditions, using four different temperatures (60, 70, 80, and 90 °C) and five relative humidities (0, 10, 20, 30, and 40%) at a constant airflow.

The higher the temperature was and the lower the RH was, the higher the rate of reduction in moisture content was. A period of constant drying rate did not occur, but the drying curves presented a falling rate period except for a very short accelerating period at the start of drying. The falling rate period was controlled by diffusion.

The Modified Oswin model and the Logarithmic model, which gave the highest values of R^2 and the lowest values of χ^2 and RSS, were the most suitable models for predicting the moisture desorption relationships and drying characteristics of tobacco strips.

Under these experimental conditions, the effective diffusion coefficient was $(1.68\text{--}6.81) \times 10^{-11} \text{ m}^2 \text{ s}^{-1}$ for C3F and $(1.62\text{--}6.68) \times 10^{-11} \text{ m}^2 \text{ s}^{-1}$ for B3F tobacco. In addition, the activation energy (E_a) values were 34.6 and 35.2 kJ/mol for C3F and B3F, respectively. A modified Arrhenius-type equation was found to be useful for describing the effect of temperature and RH on the drying of tobacco strips.

Acknowledgements The authors acknowledge the financial support of National Key Technology R&D Program of China (2015BAK39B02) and Fundamental Research Funds for the Central Universities (ZZ1327).

References

- Wang H, Xin H, Liao Z, Li J, Xie W, Zeng Q, et al. Study on the effect of cut tobacco drying on the pyrolysis and combustion properties. *Dry Technol.* 2014;32(2):130–4.
- Toğrul İT, Pehlivan D. Modelling of thin layer drying kinetics of some fruits under open-air sun drying process. *J Food Eng.* 2004;65(3):413–25.
- Kayran S, Doymaz İ. Determination of drying kinetics and physicochemical characterization of apricot pomace in hot-air dryer. *J Therm Anal Calorim.* 2017;130(2):1163–70. <https://doi.org/10.1007/s10973-017-6504-0>.
- Krokida MK, Karathanos VT, Maroulis ZB, Marinos-Kouris D. Drying kinetics of some vegetables. *J Food Eng.* 2003;59(4):391–403.
- Huang YW, Chen MQ. Thin-layer isothermal drying kinetics of municipal sewage sludge based on two falling rate stages during hot-air-forced convection. *J Therm Anal Calorim.* 2017;129(1):567–75. <https://doi.org/10.1007/s10973-017-6150-6>.
- Hosseinebadi HZ, Doosthoseini K, Layeghi M. Drying kinetics of poplar (*populus deltoides*) wood particles by a convective thin layer dryer. *Drvna Ind.* 2012;63(3):169–76.
- Esturk O. Intermittent and continuous microwave-convective air-drying characteristics of sage (*Salvia officinalis*) leaves. *Food Bioprocess Technol.* 2012;5(5):1664–73.
- Roberts JS, Kidd DR, Padilla-Zakour O. Drying kinetics of grape seeds. *J Food Eng.* 2008;89(4):460–5.
- Alvarez-López I, Llanes-Santiago O, Verdegay JL. Drying process of tobacco leaves by using a fuzzy controller. *Fuzzy Set Syst.* 2005;150(3):493–506.
- Martínezmartínez V, Baladrón C, Gomezgil J, Ruizruiz G, Navasgracia LM, Aguiar JM, et al. Temperature and relative humidity estimation and prediction in the tobacco drying process using artificial neural networks. *Sens Basel.* 2012;12(10):14004–21.
- Kiranoudis CT, Maroulis ZB, MarinosKouris D. Mass transfer modeling for virginia tobacco curing. *Dry Technol.* 1990;8(2):351–66.
- Legros R, Millington CA, Clift R. Drying of tobacco particles in a mobilized bed. *Dry Technol.* 1994;12(3):517–43.
- Zhu WK, Wang L, Duan K, Chen LY, Li B. Experimental and numerical investigation of the heat and mass transfer for cut tobacco during two-stage convective drying. *Dry Technol.* 2015;33(8):907–14.
- Liu JT, Li M, Yu QF, Ling DL. A novel parabolic trough concentrating solar heating for cut tobacco drying system. *Int J Photoenergy.* 2014;2014:1–10.
- Huang F, Chen Q, Wang L, Dou J, Wang S, Li B. Study on thin-layer dynamic models of humidifying and drying of tobacco strips. *Acta Tabacaria Sin.* 2014;20(6):34–40 (in Chinese).
- Xu D, Dai Y, Jin D, Zhu W, Du J. Effects of drying conditions on rehydration characteristics of tobacco strips. *Tob Sci Technol.* 2013(4):5–8 + 15 (in Chinese).
- Bispo JAC, Bonafe CFS, Santana KMOV, Santos ECA. A comparison of drying kinetics based on the degree of hydration and moisture ratio. *LWT Food Sci Technol.* 2015;60(1):192–8.
- Bruce DM. Exposed-layer barley drying: three models fitted to new data up to 150 °C *. *J Agric Eng Res.* 1985;32(4):337–48.
- Chen D-Y, Zhang D, Zhu X-F. Heat/mass transfer characteristics and non isothermal drying kinetics at the first stage of biomass pyrolysis. *J Therm Anal Calorim.* 2012;109(2):847–54. <https://doi.org/10.1007/s10973-011-1790-4>.
- Babalís SJ, Papanicolaou E, Kyriakis N, Belessiotis VG. Evaluation of thin-layer drying models for describing drying kinetics of figs (*Ficus Carica*). *J Food Eng.* 2006;75(2):205–14.
- Yaldiz O, Ertekin C, Uzun HI. Mathematical modeling of thin layer solar drying of Sultana grapes. *Energy.* 2001;26(5):457–65.
- Heras ML, Heredia A, Castelló ML, Andrés A. Moisture sorption isotherms and isosteric heat of sorption of dry persimmon leaves. *Food Biosci.* 2014;7:88–94.
- Raji AO, Ojediran JO. Moisture sorption isotherms of two varieties of millet. *Food Bioprod Process.* 2011;89(3):178–84.
- Kaymak-Ertekin F, Gedik A. Sorption isotherms and isosteric heat of sorption for grapes, apricots, apples and potatoes. *LWT Food Sci Technol.* 2004;37(4):429–38.
- Halsey G. Physical adsorption on non-uniform surfaces. *J Chem Phys.* 1948;16(10):931–7.
- Mehta S, Singh A. Adsorption isotherms for red chilli (*Capsicum annum L.*). *Eur Food Res Technol.* 2006;223(6):849–52.
- Zhang JW, Xin YN, Li B. Effects of temperature and humidity of drying medium on drying kinetics of strips. *Tob Sci Technol.* 2014;10:15–9 (in Chinese).
- Tahmasebi A, Yu J, Han Y, Zhao H, Bhattacharya S. A kinetic study of microwave and fluidized-bed drying of a Chinese lignite. *Chem Eng Res Des.* 2013;92(1):54–65.
- Queiroz MR, Nebra SA. Theoretical and experimental analysis of the drying kinetics of bananas. *J Food Eng.* 2001;47(2):127–32.
- Crank J. *The mathematics of diffusion.* Oxford: Clarendon Press; 1975.
- Bi J, Yang A, Liu X, Wu X, Chen Q, Wang Q, et al. Effects of pretreatments on explosion puffing drying kinetics of apple chips. *LWT Food Sci Technol.* 2015;60(2):1136–42.
- Evin D. Thin layer drying kinetics of *Gundelia tournefortii L.* *Food Bioprod Process.* 2012;90(2):323–32.
- Meziane S. Drying kinetics of olive pomace in a fluidized bed dryer. *Energy Convers Manag.* 2011;52(52):1644–9.
- Ait ML, Kouhila M, Jamali A, Lahsasni S, Mahrouz M. Moisture sorption isotherms and heat of sorption of bitter orange leaves (*Citrus aurantium*). *J Food Eng.* 2005;67(4):491–8.
- Argyropoulos D, Alex R, Kohler R, Müller J. Moisture sorption isotherms and isosteric heat of sorption of leaves and stems of lemon balm (*Melissa officinalis L.*) established by dynamic vapor sorption. *LWT Food Sci Technol.* 2012;47(2):324–31.
- Mghazli S, Idrimam A, Mahrouz M, Lahnine L, Hidar N, Ouhammou M, et al. Comparative moisture sorption isotherms, modelling and isosteric heat of sorption of controlled and irradiated Moroccan rosemary leaves. *Ind Crop Prod.* 2016;88:28–35.
- He X, Lau AK, Sokhansanj S, Lim CJ, Bi XT, Melin S, et al. Moisture sorption isotherms and drying characteristics of aspen (*Populus tremuloides*). *Biomass Bioenerg.* 2013;57(10):161–7.
- Horuz E, Bozkurt H, Karataş H, Maskan M. Drying kinetics of apricot halves in a microwave-hot air hybrid oven. *Heat Mass Transf.* 2017;53(6):2117–27.
- Beigi M. Hot air drying of apple slices: dehydration characteristics and quality assessment. *Heat Mass Transf.* 2016;52(8):1435–42.
- Aghbashlo M, Kianmehr MH, Hassan-Beygi SR. Drying and rehydration characteristics of sour cherry (*prunus cerasus l.*). *J Food Process Conserv.* 2010;34(3):351–65.
- Pusat S, Akkoyunlu MT, Erdem HH, Dağdaş A. Drying kinetics of coarse lignite particles in a fixed bed. *Fuel Process Technol.* 2015;130(130):208–13.

42. Inazu T, Iwasaki KI, Furuta T. Effect of temperature and relative Humidity on drying kinetics of fresh Japanese noodle (Udon). *LWT Food Sci Technol.* 2002;35(8):649–55.
43. Villeneuve S, Gélinas P. Drying kinetics of whole durum wheat pasta according to temperature and relative humidity. *LWT Food Sci Technol.* 2007;40(3):465–71.
44. Chen Q, Bi J, Wu X, Yi J, Zhou L, Zhou Y. Drying kinetics and quality attributes of jujube (*Zizyphus jujuba* Miller) slices dried by hot-air and short- and medium-wave infrared radiation. *LWT Food Sci Technol.* 2015;64(2):759–66.
45. Doymaz İ. Effect of pre-treatments using potassium metabisulphide and alkaline ethyl oleate on the drying kinetics of apricots. *Biosyst Eng.* 2004;89(3):281–7.
46. Toğrul İT, Pehlivan D. Modelling of drying kinetics of single apricot. *J Food Eng.* 2003;58(1):23–32.
47. Panchariya PC, Popovic D, Sharma AL. Thin-layer modelling of black tea drying process. *J Food Eng.* 2002;52(4):349–57.
48. Park KJ, Vohnikova Z, Fpr B. Evaluation of drying parameters and desorption isotherms of garden mint leaves (*Mentha crispa* L.). *J Food Eng.* 2002;51(3):193–9.
49. Kaleemullah S, Kailappan R. Drying kinetics of red chillies in a rotary dryer. *Biosyst Eng.* 2005;92(1):15–23.
50. Kaleemullah S, Kailappan R. Modelling of thin-layer drying kinetics of red chillies. *J Food Eng.* 2006;76(4):531–7.
51. Ortiz J, Lemus-Mondaca R, Vega-Gálvez A, Kong AH, Puente-Diaz L, Zura-Bravo L, et al. Influence of air-drying temperature on drying kinetics, colour, firmness and biochemical characteristics of Atlantic salmon (*Salmo salar* L.) fillets. *Food Chem.* 2013;139(1–4):162–9.
52. Demiray E, Tulek Y. Drying characteristics of garlic (*Allium sativum* L) slices in a convective hot air dryer. *Heat Mass Transf.* 2014;50(6):779–86.
53. Doymaz İ. Thin-layer drying characteristics of sweet potato slices and mathematical modelling. *Heat Mass Transf.* 2011;47(3):277–85.